JVI Journals.ASM.org

Nucleolar Trafficking of the Mouse Mammary Tumor Virus Gag Protein Induced by Interaction with Ribosomal Protein L9

Andrea R. Beyer,[a]* Darrin V. Bann,[b] Breanna Rice,[b] Ingrid S. Pultz,[c,d] Melissa Kane,[e]* Stephen P. Goff,[f] Tatyana V. Golovkina,[c,e] Leslie J. Parent[a,b]

Departments of Microbiology and Immunology[a] and Medicine,[b] Pennsylvania State University College of Medicine, Hershey, Pennsylvania, USA; Jackson Laboratory, Bar Harbor, Maine, USA[c]; Department of Biochemistry, University of Washington, Seattle, Washington, USA[d]; Department of Microbiology, University of Chicago, Chicago, Illinois, USA[e]; Departments of Biochemistry and Molecular Biophysics and Microbiology and Immunology, Howard Hughes Medical Institute, Columbia University, New York, New York, USA[f]

The mouse mammary tumor virus (MMTV) Gag protein directs the assembly in the cytoplasm of immature viral capsids, which subsequently bud from the plasma membranes of infected cells. MMTV Gag localizes to discrete cytoplasmic foci in mouse mammary epithelial cells, consistent with the formation of cytosolic capsids. Unexpectedly, we also observed an accumulation of Gag in the nucleoli of infected cells derived from mammary gland tumors. To detect Gag-interacting proteins that might influence its subcellular localization, a yeast two-hybrid screen was performed. Ribosomal protein L9 (RPL9 or L9), an essential component of the large ribosomal subunit and a putative tumor suppressor, was identified as a Gag binding partner. Overexpression of L9 in cells expressing the MMTV(C3H) provirus resulted in specific, robust accumulation of Gag in nucleoli. Förster resonance energy transfer (FRET) and coimmunoprecipitation analyses demonstrated that Gag and L9 interact within the nucleolus, and the CA domain was the major site of interaction. In addition, the isolated NC domain of Gag localized to the nucleolus, suggesting that it contains a nucleolar localization signal (NoLS). To determine whether L9 plays a role in virus assembly, small interfering RNA (siRNA)-mediated knockdown was performed. Although Gag expression was not reduced with L9 knockdown, virus production was significantly impaired. Thus, our data support the hypothesis that efficient MMTV particle assembly is dependent upon the interaction of Gag and L9 in the nucleoli of infected cells.

Since its discovery as a milk-transmitted agent in the 1930s, the oncogenic retrovirus mouse mammary tumor virus (MMTV) has served as an important model in breast cancer research and immunology (1). However, little is known about the molecular mechanisms that govern MMTV assembly. The 9-kb MMTV RNA genome consists of the common retroviral elements *gag*, *pro*, *pol*, and *env*, as well as *dut* (dUTPase) (2), *sag* (superantigen) (3), and *rem* (regulator of export of MMTV mRNA) (4, 5). Like all retroviruses, MMTV uses full-length viral RNA to transcribe the viral structural proteins Gag, Gag-Pro, and Gag-Pro-Pol. The Gag protein directs assembly of complete, immature viral capsids in the cytoplasm, which are subsequently transported to the plasma membrane for release by budding.

Unlike acutely transforming retroviruses like Rous sarcoma virus (RSV), MMTV does not carry an oncogene and instead induces tumors primarily by integrating near cellular oncogenes and disrupting their regulation. In addition, the MMTV Gag and Env proteins also promote tumorigenesis independently of the proviral integration site (6, 7). Moreover, differences in pathogenesis between the highly tumorigenic MMTV(C3H) strain and the tumor-attenuated MMTV hybrid provirus (HP) strain map to the CA and NC regions of the Gag protein (6), which led us to hypothesize that the Gag proteins from the C3H and HP strains might differentially interact with cellular proteins to promote malignant transformation.

The eukaryotic ribosome serves as the catalytic and regulatory center of cellular protein synthesis and is a key player in many aspects of cell and structural biology. It consists of two subunits, the 60S large subunit and the 40S small subunit, which interact noncovalently to mediate the translation of mRNA into polypeptide products. The large subunit contains the 25S, 5.8S, and 5S rRNAs, in addition to more than 45 proteins (8), including RPL9 (L9), a 192-amino-acid protein (9) present in a single copy within the ribosome (10). L9 plays an important role in proper ribosome formation and in normal growth and development. *Drosophila melanogaster* mutants carrying one defective *rpL9* allele are characterized by stunted growth, reduced viability, and diminished fertility; homozygosity of the mutated gene is lethal (11). Homozygous mutations of *rpL9* are also embryonic lethal in zebrafish (12), emphasizing the necessity of L9 for viability and early development. The crystal structure of L6, the prokaryotic equivalent of eukaryotic L9, provides the basis for structural information on the protein, which consists of two domains with nearly identical folds that may have arisen from an ancient gene duplication event (13). The structure suggests that the N terminus participates in protein-protein interactions at the interface between the large and small ribosomal subunits, while the C-terminal hydrophobic residues bind the 28S rRNA within the interior of the ribosome (13). In the canine ribosome, a small portion of L9 is visible on the large-subunit surface (8), which is presumably the N terminus at the

Received 14 September 2012 Accepted 1 November 2012
Published ahead of print 7 November 2012
Address correspondence to Leslie J. Parent, lparent@psu.edu.
* Present address: Andrea R. Beyer, Department of Microbiology and Immunology, Virginia Commonwealth University School of Medicine, Richmond, Virginia, USA; Melissa Kane, Aaron Diamond AIDS Research Center, New York, New York, USA.
A.R.B. and D.V.B. contributed equally to this work.

doi:10.1128/JVI.02463-12

subunit boundary. Use of trypsin digestion to remove ribosomal proteins located on the surface of the large ribosome subunit failed to remove L9, indicating that it is positioned more internally on the 60S subunit than other ribosomal proteins (14).

Here, we report the unexpected finding that L9 interacts with the MMTV Gag protein in cells infected with MMTV(C3H) virus, a highly tumorigenic strain. Our data indicate that MMTV Gag and L9 interact in the nucleolus, a subnuclear body involved in ribosome biogenesis, cell cycle control, DNA damage responses, and the p53 regulatory feedback loop (reviewed in references 15 and16). Interestingly, small interfering RNA (siRNA)-mediated knockdown of L9 reduced L9 expression in the nucleolus, and the MMTV yield was also reduced without affecting steady-state levels of the Gag protein. Together, these data suggest that MMTV Gag interacts with extraribosomal L9 during the process of virus assembly.

MATERIALS AND METHODS

Plasmids. pRPL4-GFP and pRPS6-GFP (17) (kind gifts from Tim Krüger, University of Würzburg, Würzburg, Germany), pRSV Gag-GFP (18), and pGFP-Rem (5) were previously described. pFibrillarin-GFP (19), a kind gift of Mark Olson (University of Mississippi Medical Center), was modified using PCR cloning to exchange cyan fluorescent protein (CFP) for green fluorescent protein (GFP). pRPL9-FLAG was cloned by amplification of murine *rpL9* from total cellular RNA from NMuMG cells using PCR (NCBI NM_011292) and inserted into the BglII site of the pCMV-FLAG-MAT-2 vector (Sigma). pRPL9-mCherry was created by inserting the RPL9 sequence from RPL9-FLAG into pmCherry.N2, which was made by replacing GFP in pEGFP.N2 (Clontech) with mCherry from pRSet8.mCherry, a kind gift of Roger Tsien (University of California, San Diego) (20). pRPL9-GFP was made by amplification of RPL9 from RPL9-FLAG and insertion into the HindIII/SalI sites of pEGFP.N2. pMMTV.Gag(C3H)-GFP was created by PCR amplification of the MMTV(C3H) *gag* sequence (6) from plasmid pRFPC-Bait-C used in the yeast two-hybrid assay described below [nucleotide sequence accession number AF228552 for MMTV(C3H) provirus] and insertion into pEGFP.N2 using BamHI-HindIII; 21 nucleotides of the 5′ untranslated region (UTR) upstream of Gag were included in the construct. Similarly, pMMTVGag(C3H)-mCherry was made by PCR amplification of C3H Gag and insertion into mCherry.N2 using the HindIII/ApaI sites.

GFP-tagged MMTV(C3H) Gag truncation proteins MA-CA (1 to 1485) and CA (805 to 1485) were PCR amplified at the indicated nucleotides of *gag* and ligated into the BamHI-HindIII restriction sites of pEGFP.N2. The NC coding region of *gag* (1486 to 1767) was PCR amplified, digested with BglII, treated with Klenow, digested with BamHI, and ligated into pEGFP.N2 to produce pNC-GFP. pYRPL9B-mCherry was made by amplification of *rpL9* isoform B sequences (http://www.yeastgenome.org; YNL067W) from *Saccharomyces cerevisiae* genomic cDNA (a kind gift from Anita Hopper, Ohio State University) and insertion into pmCherry.N2 using HindIII-SalI. pRPL9.NT-mCherry (1 to 255) and pRPL9.CT-mCherry (256 to 576) were made by PCR amplification of the indicated *rpL9* nucleotide bases and ligated into pmCherry using HindIII-SalI.

The sequence encoding the nucleolar localization signal (NoLS) of HIV-1 Rev (21) (NCBI K03455) was amplified from pRev-YFP and cloned into pmCherry or pRPL9.CT-mCherry via SalI-ApaI. pRev-YFP was made by amplifying Rev from pCMV-Rev (a kind gift from Bryan Cullen, Duke University) (22, 23) and transferring it into SalI-ApaI of pEYFP.N2. All plasmid constructs were sequenced and shown to be faithful copies of the corresponding genes. The primer sequences of all oligonucleotides used for cloning are available upon request.

Yeast-two hybrid (Y2H) analysis. BALB/cJ and C3H/HeN lactating mammary gland cDNA libraries were used to clone DNAs into the pGADNOT vector (24) to produce GAL4-cDNA activation domain fusion preys. Over 300,000 GAL4-cDNA plasmid clones were made, representing each mouse genome gene with 10-fold redundancy. The *Mtv1 gag* and MMTV(C3H) *gag* sequences were also cloned into the pGADNOT vector to serve as Gag-Gag homodimerization positive controls. The MMTV(C3H) *gag*, *Mtv1 gag*, and chimeric *gag* genes were cloned upstream of LexA in the pNLexA vector (OriGene Technologies, Inc.) to create Gag-LexA binding domain fusion baits. p*gag*MMTV(C3H)-LexA and a cDNA library were transformed into CTY10-5d yeast cells (*MAT***a** *ade2 trp-901 leu2-3,112 his3-200 gal4*$^{-}$ *gal80 URA3*::*lexA-LacZ*) to identify interactors. Interacting clones were tested for the ability to bind to MMTV(C3H) Gag and *Mtv1* Gag in the Y2H assay, and only one, RPL9 (L9), was found to interact with MMTV(C3H) Gag preferentially compared to *Mtv1* Gag. L9 was identified three independent times (twice from the C3H/HeN library and once from the BALB/cJ library). Positive protein interactions between bait and prey were measured with beta-galactosidase activity on X-Gal (5-bromo-4-chloro-3-indolyl-β-D-galactopyranoside) plates. Quantification of protein-protein interactions was performed by using the β-Gal liquid assay on permeabilized yeast, as described previously (25).

Cell culture and transfection. NMuMG (normal murine mammary gland) cells (ATCC CRL-1636), MMTV(C3H)-infected NMuMG cells (26, 27), and NMuMG-MM5MT cells were cultured in Dulbecco's modified Eagle's medium (DMEM) supplemented with 10% fetal bovine serum, penicillin, streptomycin, and amphotericin B (HyClone). NMuMG cells infected with MMTV(C3H) were made either by transfection of the proviral plasmid pHPA [cells designated NMuMG(C3H)] or by coculture with MM5MT cells (28) derived from MMTV(C3H)-infected mammary gland tumor cells of a C3H/He-infected mouse (cells designated NMuMG-MM5MT). After 1 week of coculture, newly infected NMuMG cells (which carry a stable integration of the hygromycin resistance gene) were selected by treatment with hygromycin. NMuMG cells were transfected using Lipofectamine 2000 (Invitrogen) according to the manufacturer's directions. For coculture infections, 1.5×10^4 NMuMG and 0.5×10^4 NMuMG-MM5MT (ATCC CRL-1637) cells were cocultured for 24 h in an 8-well Lab-Tek II chamber slide (Nunc). Quail fibroblast (QT6) cells were cultured as previously described (29) and transfected via the calcium phosphate method.

Microscopic imaging. Cells were seeded in 35-mm dishes containing glass coverslips, fixed in 4% paraformaldehyde, washed in phosphate-buffered saline (PBS), permeabilized with 0.25% Triton X-100–PBS, and blocked with 10% bovine serum albumin (BSA)-PBS. The primary antibodies used were mouse anti-MMTV CA (30), mouse anti-FLAG (Sigma), or rabbit anti-RPL9 (AbCam). After washing in PBS, the coverslips were incubated with sheep anti-mouse IgG-Cy3 (Sigma), goat anti-mouse IgG-Cy3 (Sigma), goat anti-mouse IgG-fluorescein isothiocyanate (FITC) (Sigma), goat anti-mouse IgG-Alexa Fluor 514 (Invitrogen), or goat anti-rabbit IgG-Cy5 (AbCam). Cell nuclei were stained with DAPI (4′,6-diamidino-2-phenylindole), and SlowFade reagent (Molecular Probes) was used for mounting coverslips. The fixed cells were examined using a Leica AOBS SP2 confocal microscope or a DeltaVision DV Elite deconvolution microscope (Applied Precision) and deconvolved using softWoRx 2.0 software. Cell images were false colored using ImageJ (version 1.41o; Wayne Rasband, NIH [31]), and image intensities were adjusted uniformly using CorelDRAW X3 (version 13; Corel Corp). Colocalization scores using Mander's overlap coefficient (M_1 and M_2) as modified by Bolte and Cordelieres (32) were calculated for individual transfected cells representative of the population of cells using Just Another Colocalization Plugin (JACoP) for ImageJ. M_1 represents the proportion of the green signal coincident with a signal in the red channel over its total intensity and M_2 represents the converse for the red channel (32). Thresholds were set to remove the background signal while remaining representative of the confocal image.

For cells infected by coculture, cells were fixed using 4% paraformaldehyde in PBS for 15 min, permeabilized with 0.2% Triton X-100, blocked with 30% sheep serum, incubated with primary and secondary antibodies,

and mounted on DAPI-containing mounting medium (Invitrogen). MMTV Gag was detected using the mouse monoclonal anti-p27CAGag antibody (30), followed by donkey anti-mouse AlexaFluor 568 (Invitrogen) secondary antibody. Cells were viewed with the 100× or 63× objective lens of a Nikon A1 confocal microscope and captured with NIS Elements software (Nikon Inc.).

Acceptor photobleaching (AP)-FRET analysis. Using fixed and immunostained cells, prebleach images were obtained for GFP (excitation at 488 nm; emission at 492 to 533 nm; 25% laser power) or mCherry (excitation at 543 nm; emission at 558 to 599 nm; 50% laser power) channels using sequential scanning. For photobleaching, nuclei were selected as the region of interest, and mCherry was photobleached using the 543-nm laser at 100% power until the fluorescence intensity was reduced to 20% of prebleach levels or for 5 min. Förster resonance energy transfer (FRET) efficiency was calculated as previously described (33). FRET analysis was performed using a minimum of 10 different cells on two different days, and the mean, standard error of the mean, and *P* values were calculated using an unpaired *t* test with GraphPad Prism 5 (GraphPad Software, Inc.).

Coimmunoprecipitation. MMTV-infected NMuMG(C3H) cells were harvested in PBS, incubated in lysis buffer (50 mm Tris, pH 7.05, 1% Triton X-100, 0.5% deoxycholic acid, 150 mM NaCl) for 15 min on ice, and spun for 30 min in a 4°C microcentrifuge at maximum speed to pellet debris. The protein concentration of the cleared lysate was determined by Bradford assay. Protein A Sepharose beads (Invitrogen) were washed twice in coimmunoprecipitation (coIP) buffer (50 mM Tris, pH 8.0, 1% Triton X-100, 0.1% SDS, 1% deoxycholic acid, 150 mM NaCl) and incubated with one of the following antibodies in coIP buffer for 1 h: goat anti-CA (a kind gift from Susan Ross, University of Pennsylvania), goat anti-lamin B (Santa Cruz), rabbit anti-RPL9 (AbCam), or rabbit anti-lamin A/C (Santa Cruz). The antibody-bound beads were added to 1.5 mg of total cellular protein per coIP, and the reaction mixtures were incubated at 4°C overnight. Precipitated beads were washed twice with coIP buffer, followed by two washes in TE (10 mM Tris-HCl, pH 7.5, 1 mM EDTA, pH 8.0). Proteins were eluted by boiling in 2× SDS loading dye (125 mM Tris-HCl, pH 6.8, 20% glycerol, 0.5% bromophenol blue, 4% SDS, and 10% β-mercaptoethanol) prior to analysis by SDS-PAGE and Western blotting.

L9 siRNA-mediated knockdown and virus yield assays. Cells were seeded in 35-mm dishes at a density of 0.25×10^6 cells/dish. Twenty-four hours after seeding, the cells were transfected with L9 Smartpool siRNA (Dharmacon; M-042220-01-0005) or scrambled control siRNA (Sigma) for 15 h using Lipofectamine 2000 according to the manufacturer's instructions. The cells were washed once in standard buffer (100 mM NaCl, 10 mM Tris, 1 mM EDTA, pH 7.2) and allowed to recover in primary growth medium for 9 h. The cells were then transfected a second time with L9 or control siRNA for 15 h. After the second transfection, the cells were washed three times in standard buffer, and virus was collected for 3 h in primary growth medium. The medium was removed from the cells and cleared by centrifugation at 2,000 × *g* at 4°C, layered onto a 25% sucrose cushion, and pelleted by centrifugation at 126,000 × *g* at 4°C. The pelleted viral particles were resuspended in RIPA buffer (50 mM Tris, pH 7.5, 150 mM NaCl, 1% NP-40, 0.5% deoxycholate, 0.1% SDS). The cells were washed in standard buffer and lysed in RIPA buffer. The protein concentration of cell lysates was determined by Bradford assay, and normalized amounts were loaded onto an SDS-PAGE gel.

Virus yield and L9 expression were determined by Western blotting using the following antibody combinations: mouse anti-MMTV CA with goat anti-mouse-horseradish peroxidase (HRP) (Sigma), rabbit anti-RPL9 (AbCam) with goat anti-rabbit-HRP (Sigma), or goat anti-GAPDH (glyceraldehyde-3-phosphate dehydrogenase) (GenScript) with rabbit anti-goat-HRP (Sigma). Blots were developed using SuperSignal West Pico Chemiluminescent substrate (Thermo Scientific) and imaged using an EC3 Chemi HR 410 imaging system (UVP, Upland, CA). The virus yield was calculated as the amount of viral protein detected in the sucrose-purified medium divided by the sum of viral proteins in the lysate plus medium [medium/(lysate + medium)]. L9 expression was normalized to GAPDH loading controls to calculate the relative knockdown of expression. Virus yield assays were performed a minimum of seven times for each condition. The mean, standard error of the mean, and *P* values were calculated using GraphPad Prism 5 (GraphPad Software, Inc.).

RESULTS

We previously described a group of replication-competent exogenous MMTV strains that differ in their propensities to cause tumors in mice (6, 34). Compared to the highly tumorigenic strain MMTV(C3H), a tumor-attenuated virus was identified that arose from a recombination event between MMTV(C3H) and an endogenous retrovirus, *Mtv1*, to create the MMTV(HP/*Mtv1*) strain (6, 34). The difference in tumorigenicity between the MMTV(C3H) and MMTV(HP/*Mtv1*) strains of exogenous MMTV maps to a 253-amino-acid region within the CA and NC regions of Gag (6).

Yeast two-hybrid screen. To identify cellular proteins that might play a role in MMTV Gag-mediated tumorigenesis, a yeast two-hybrid screen was used to identify host proteins that differentially interacted with MMTV(C3H) or MMTV(HP/*Mtv1*) Gag. As bait, we used a series of hybrid Gag proteins that contained replacements of the tumor-attenuated MMTV(HP/*Mtv1*) *gag* sequence with corresponding regions from the highly tumorigenic MMTV(C3H) *gag* gene (Fig. 1A) (34). cDNA libraries made from the mammary glands of C3H/HeN and BALB/cJ mice were used as prey. L9 was the only protein found to interact more strongly with Gag proteins derived from viruses with higher tumor incidence (virus A [virA] and virus C [virC]) than with tumor-attenuated viruses (HP/*Mtv1* and virus B [virB]) (Fig. 1B, right). Quantitation of the Gag-L9 interactions revealed the highest degree of binding between virA Gag and L9, while virC Gag demonstrated intermediate binding. The virB and *Mtv1* Gag proteins produced the weakest interactions (Fig. 1C). The observation that the strength of the interaction between Gag and L9 in yeast cells was correlated with the tumorigenicity of the virus led us to investigate whether L9 and MMTV Gag interacted in cultured mouse mammary (NMuMG) cells. To this end, we first examined the subcellular localizations of L9 and the Gag protein of MMTV(C3H), which is identical to that of *gag*virA used in the yeast two-hybrid analysis (Fig. 1) (34).

Cell line-specific localization of MMTV Gag to nucleoli. In mouse mammary cells stably transfected with an MMTV(C3H) proviral expression vector (NMuMG-C3H), Gag formed discrete cytoplasmic foci with exclusion of the nucleus when imaged using deconvolution microscopy (Fig. 2A, top row, yellow arrow). In contrast, we were surprised to find a population of Gag that localized to nucleoli in NMuMG cells infected by coculture with MMTV(C3H)-infected MM5MT cells isolated from mouse tumors (NMuMG-MM5MT) (Fig. 2A, bottom row, and B, yellow arrows). In addition, cells newly infected by coculture with NMuMG-MM5MT cells also revealed Gag within nucleoli (Fig. 2B, white arrows), indicating that Gag localized to nucleoli in cells newly infected via cell-to-cell spread.

L9 is a component of the large ribosomal subunit (35, 36). In NMuMG cells, endogenous L9 was localized to the cytoplasm and to nucleoli, the site of preribosome assembly and where L9 colocalized with fibrillarin-CFP (Fig. 2C, top row, yellow arrow). We also noticed that the L9 antibody stained mitotic spindles in di-

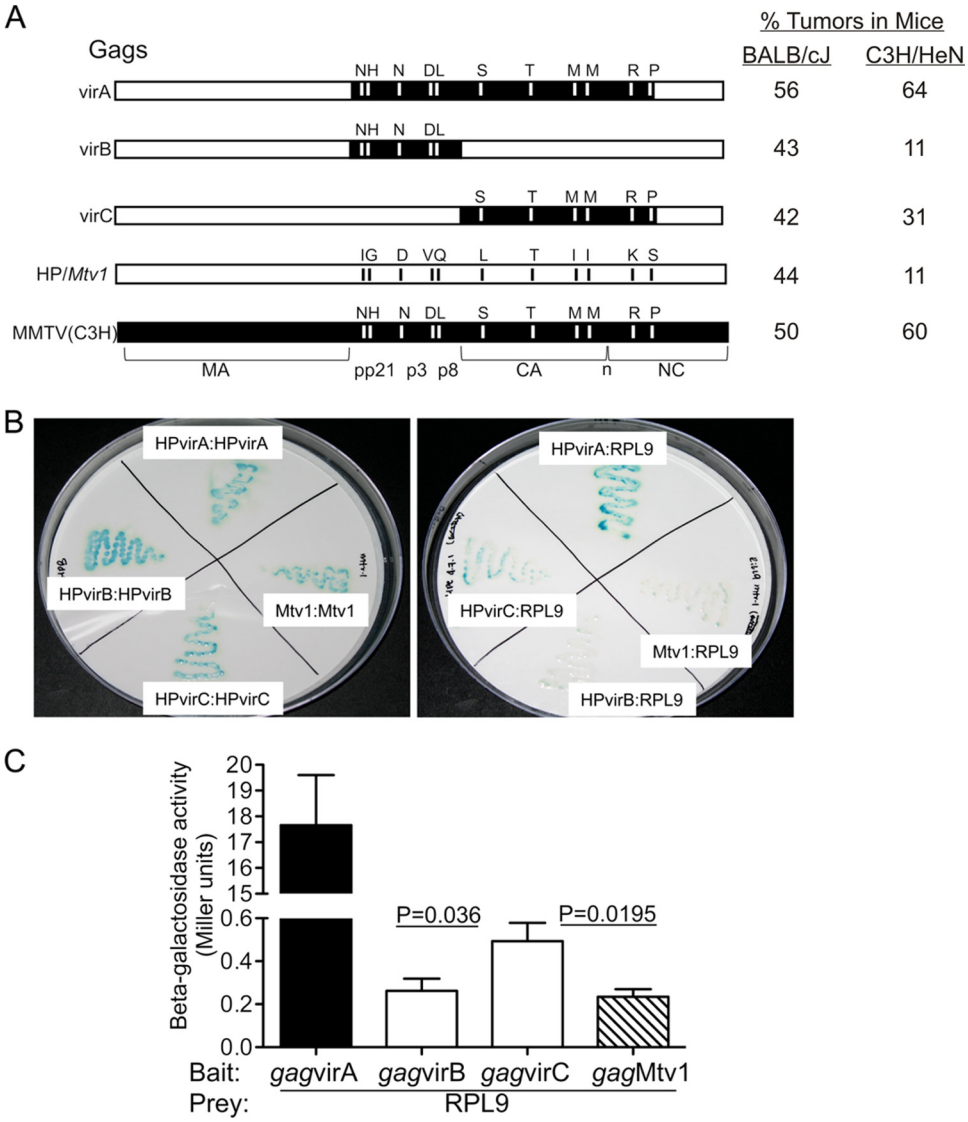

FIG 1 Yeast two-hybrid screen implicating L9 as an MMTV Gag binding partner. (A) Comparison of Gag sequences of chimeric viruses and parental Gag constructs derived from *Mtv1* and MMTV(C3H). Differences between *gag* gene products are indicated by vertical bars, and the amino acids are shown at each position. Gag cleavage products are indicated below the schematic diagram of MMTV(C3H) Gag: MA, pp21, p3, p8, n, CA, and NC. The tumorigenic potential of the viruses carrying the respective Gag proteins in BALB/cT and C3H/HeN mice are indicated, as previously reported by Swanson et al. (34). (B) Photographs of plates containing yeast cells transformed with pNLexAGag and pGADNOTGag (positive controls) (left) or with pGADNOT RPL9 and pNLexAGag (right). Positive protein-protein interactions result in blue colonies. (C) Quantitation of the beta-galactosidase activity of the Gag-RPL9 interactions. An unpaired *t* test was applied to determine the *P* value. The error bars indicate standard deviations.

viding cells, a finding that had not been reported previously (Fig. 2C, bottom row). Based on the observation that a subpopulation of Gag was localized in the nucleoli of NMuMG-MM5MT cells, we tested whether L9 overexpression would alter Gag localization in NMuMG-C3H cells. To differentiate transfected L9 from the endogenous protein, we created epitope (FLAG)- or fluorophore (GFP or mCherry)-tagged L9 constructs. As expected, L9-mCherry colocalized with fibrillarin-CFP in nucleoli of NMuMG cells (Fig. 2D, top row). Interestingly, when L9 was overexpressed in NMuMG-C3H cells, Gag (detected using an α-CA antibody) accumulated in nucleoli in 78% of the cells ($n = 23$) overexpressing L9-mCherry (Fig. 2D, bottom row). Colocalization analysis of the cells where Gag was relocalized by L9-mCherry expression revealed that, on average, 18% ± 4% of the Gag signal colocalized with L9 (M_1) and 55% ± 5% of the L9 signal colocalized with Gag (M_2) ($n = 18$) (Fig. 2D, bottom row), suggesting that L9 overexpression induced Gag to accumulate in nucleoli in NMuMG-C3H cells.

Finding a difference in the localization of Gag in NMuMG-C3H versus NMuMG-MM5MT cells was unexpected because the Gag proteins expressed in these cells are identical, as confirmed by isolation of total cellular RNA from both cell lines and sequencing of the *gag* gene using reverse transcription (RT)-PCR (data not shown). Thus, the variation in Gag localization may be due to a difference in a cellular factor or a viral component other than Gag. Although it was feasible that NMuMG-MM5MT cells might ex-

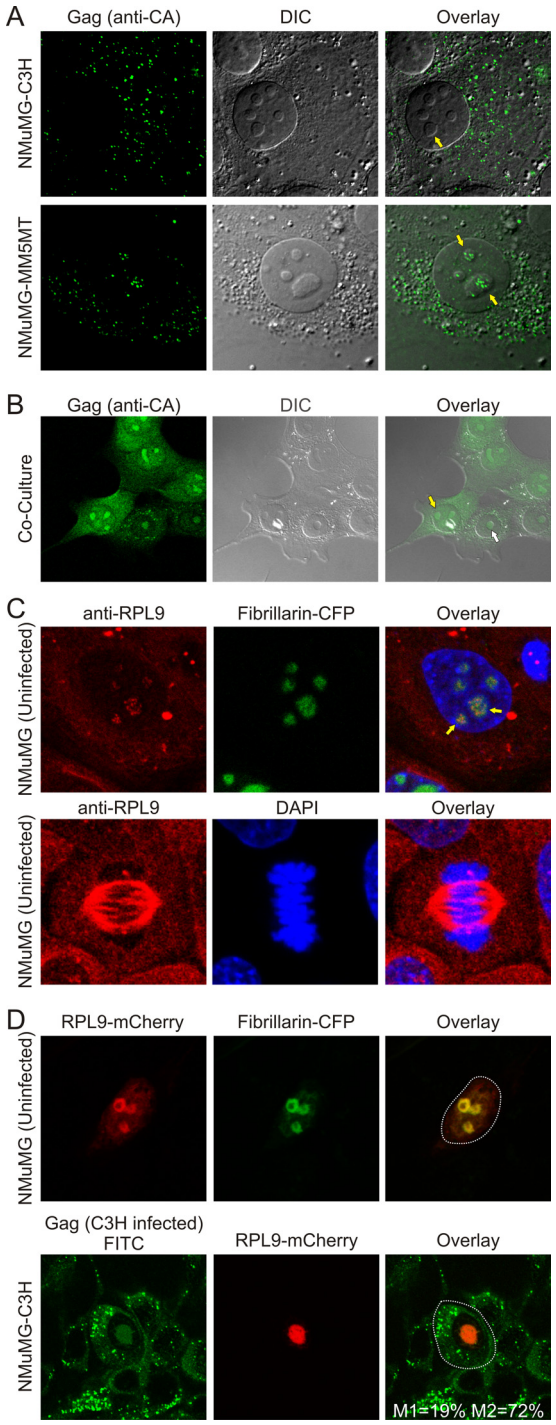

FIG 2 Localization of MMTV Gag and L9 in mouse mammary cells. (A) MMTV-infected NMuMG-C3H or NMuMG-MM5MT cells were immunostained for Gag using an anti-CA primary antibody and a secondary FITC-conjugated antibody (green) and imaged using fluorescence deconvolution microscopy. Nucleoli were identified by DIC images (yellow arrows). (B) Uninfected NMuMG cells were infected with MMTV by coculture with NMuMG-MM5MT cells, immunostained for Gag (green), and imaged using fluorescence deconvolution microscopy. Nucleoli were identified by DIC images. The yellow arrow indicates nucleolar Gag signal in NMuMG-MM5MT cells, and the white arrow points to Gag in nucleoli of newly infected cells (24 h postinfection). (C) (Top) Confocal microscopic images of NMuMG cells expressing the nucleolar protein fibrillarin-CFP (false colored green), immunostained using an anti-L9 primary antibody with a Cy5-conjugated secondary antibody (red) and stained using DAPI (blue) to show nuclei. The yellow arrows point to L9 staining within nucleoli. (Bottom) Mitotic spindle stained with anti-L9 antibody. (D) (Top) Representative NMuMG cell coexpressing fibrillarin-CFP (false colored green) and RPL9-mCherry (red) with colocalization (yellow) shown in the overlay image. The dotted line indicates the outline of the cell. (Bottom) Expression of RPL9-mCherry (red) in NMuMG-C3H cells immunostained for Gag (green). M_1 and M_2 colocalization coefficients were measured by Mander's analysis using ImageJ JACoP as described in Materials and Methods and are shown for the representative cell outlined with a white dotted line. M_1 indicates the percentage of fluorescence in the green channel that is colocalized with signal in the red channel, and M_2 is the converse.

press higher basal levels of L9 than NMuMG-C3H cells as an explanation for the nucleolar localization of Gag in NMuMG-MM5MT cells, we did not observe a significant difference in L9 levels by Western blotting (data not shown). Therefore, either the Western analysis was insufficiently sensitive to detect differences in L9 levels or a host factor in addition to L9 contributes to Gag nucleolar localization.

To test whether Gag would relocalize to nucleoli with L9 overexpression in the absence of other viral factors, we created GFP- and mCherry-tagged MMTV(C3H) Gag constructs (Gag-GFP and Gag-mCherry, respectively) (Fig. 3A). Gag-GFP and Gag-mCherry formed small cytoplasmic foci in uninfected NMuMG cells, which were similar in size and distribution to Gag foci observed in NMuMG-C3H cells (Fig. 2A). When fluorophore-tagged Gag and L9 constructs were cotransfected into uninfected NMuMG cells, Gag accumulated in nucleoli in 66% of cotransfected cells ($n = 33$) (Fig. 3B, yellow arrow). Among cells where Gag was relocalized by L9 expression, 16% ± 3% of Gag colocalized with L9 and 71% ± 3% of L9 colocalized with Gag ($n = 22$). Similar results were observed when Gag-GFP was cotransfected with FLAG-tagged L9 (L9-FLAG) (Fig. 3B, yellow arrow). Thus, the subcellular distribution of MMTV Gag was altered by L9 expression in the absence of any additional viral proteins or the viral genome. Because of the higher degree of binding in the two-hybrid assay between L9 and MMTV(C3H) Gag compared to MMTV(HP/*Mtv1*), we tested whether L9 overexpression would change the localization of Gag derived from *Mtv1*. In fact, L9 overexpression also induced localization of a subpopulation of *Mtv1* Gag to nucleoli (data not shown), indicating that the difference in binding affinity observed in the quantitative yeast two-hybrid assay was not apparent in NMuMG cells, which are derived from Namru mice (37–39). It is possible that Namru mice, like BALB/cJ mice, do not exhibit differences in the rates of tumor formation with variants of MMTV tested by Swanson et al. (34) (Fig. 1). Therefore, future experiments will need to be performed in mammary cells derived from BALB/cJ mice to address whether L9 interacts preferentially with MMTV(C3H) Gag compared with *Mtv1* Gag. In this report, we instead focused on characterizing the interaction of L9 with MMTV(C3H) Gag to learn more about its relevance to virus assembly.

To determine whether L9-induced relocalization of Gag was unique to MMTV, the GFP-tagged RSV Gag protein was cotransfected with murine RPL9-mCherry in quail fibroblasts. Overexpression of RPL9-mCherry did not affect the subcellular distribution of RSV Gag (Fig. 3C), suggesting that the interaction between Gag and L9 was limited to MMTV. To examine whether the relocalization of MMTV Gag could be induced by overexpression of

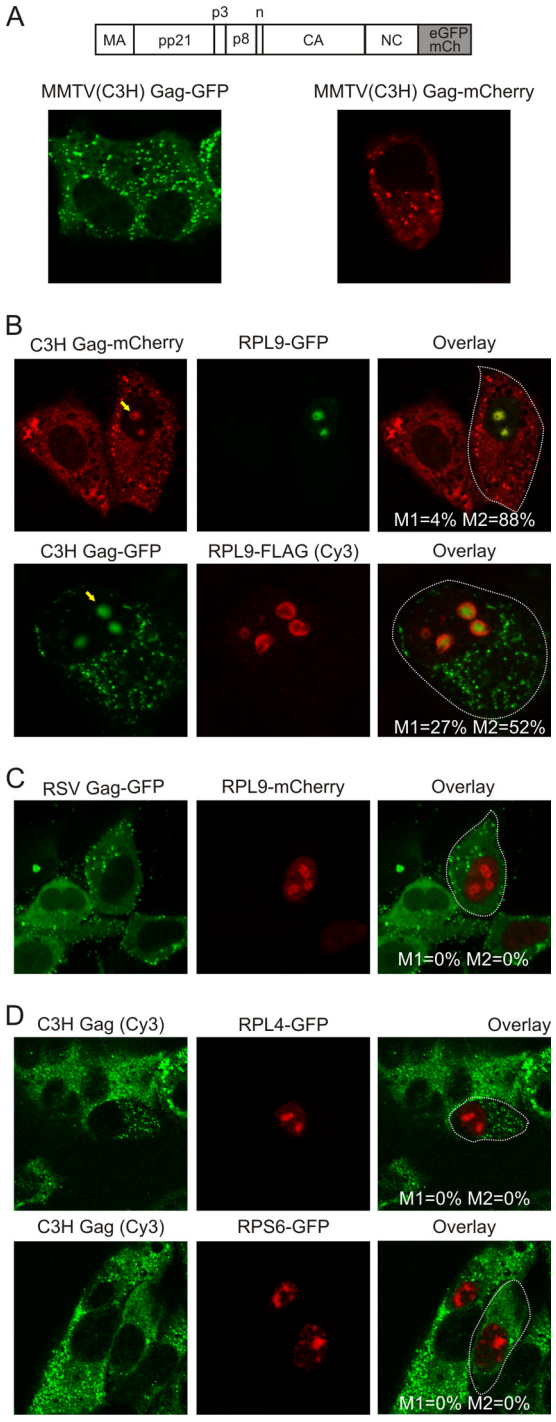

FIG 3 MMTV Gag specifically interacts with RPL9. (A) (Top) Diagram of MMTV Gag-GFP showing the cleavage sites of Gag (MA, pp21, P3, p8, n, CA, and NC). (Bottom) Expression of fluorophore-tagged MMTV Gag in uninfected NMuMG cells imaged using confocal microscopy. (B) Coexpression of MMTV Gag-mCherry with RPL9-GFP (top row) and MMTV Gag-GFP with RPL9-FLAG (bottom row) in uninfected NMuMG cells. Mander's coefficient for colocalization is shown for the representative cell outlined with a white dotted line, as described in the legend to Fig. 2. (C) RSV Gag-GFP was coexpressed with RPL9-mCherry in QT6 cells. Mander's coefficient for colocalization is shown for the representative cell outlined with a white dotted line. (D) RPL4-GFP or RPS6-GFP was expressed in MMTV-infected NMuMG-C3H cells immunostained for Gag (green). Mander's coefficient for colocalization was measured on the cell outlined with a white dotted line.

other ribosomal proteins, RPS6 and RPL4, each fused to GFP, were expressed in NMuMG-C3H cells. Both RPS6-GFP and RPL4-GFP localized to nucleoli, similarly to L9; however, MMTV Gag distribution was unaffected by S6 or L4 overexpression (Fig. 3D). Together, these data indicate that MMTV Gag specifically interacted with L9 and that this interaction may not be conserved among other retroviruses.

Gag interacts with L9 in nucleoli. To this point, our data demonstrated that although Gag was not visualized in nucleoli of NMuMG-C3H cells under steady-state conditions, overexpression of L9 induced a subpopulation of Gag to accumulate within nucleoli. To assess whether the association of Gag and L9 could be detected biochemically, we conducted coIP experiments using anti-CA or anti-RPL9 antibodies to isolate protein complexes from NMuMG-C3H cells. MMTV Gag was coimmunoprecipitated using an anti-RPL9 antibody, but not a nonspecific isotype control antibody (anti-lamin A/C IgG) (Fig. 4A, top). Similarly, a reciprocal experiment demonstrated that L9 was pulled down with an anti-CA antibody, but not with the nonspecific control antibody (anti-lamin B IgG) (Fig. 4A, bottom). It is likely that the L9 band ran higher in the immunoprecipitation lane than the unbound lanes due to differences in the salt concentrations of the samples, which may noticeably alter the electrophoretic properties of the 21-kDa L9 protein. Furthermore, Gag also coimmunoprecipitated with L9 from concentrated preparations of nucleoli (data not shown). Together, these data demonstrate that Gag and L9 form an intracellular complex in MMTV-infected mammary cells.

Next, we used AP-FRET to determine whether Gag and L9 were interacting directly within nucleoli. As we observed previously, expression of RPL9-mCherry resulted in Gag accumulation in nucleoli of MMTV-infected NMuMG-C3H cells, which were immunostained for Gag using anti-CA (α-CA) antibody and FITC-labeled secondary antibody (Fig. 4B). Photobleaching of nucleolar RPL9-mCherry with a 543-nm laser resulted in decreased mCherry fluorescence (Fig. 4B, compare top row, pre- and postbleach images, white arrows) with a concomitant increase in FITC fluorescence (compare bottom row, pre- and postbleach images, yellow arrows), indicating a significant intermolecular transfer of resonance energy between the FITC and mCherry chromophores, which was clearly visible in the images. The mean AP-FRET efficiency between FITC-stained Gag and RPL9-mCherry was 67.9% ± 13% (Fig. 4D). Because FRET occurs only when fluorophores are in very close proximity (i.e., <50 Å for enhanced GFP [EGFP] and mCherry) (40), these data suggest that Gag and L9 bind to each other within nucleoli. As a control for the FRET experiment, RPL9-mCherry was coexpressed with MMTV GFP-Rem, which also localizes to nucleoli (5) (Fig. 4C). In this case, RPL9-mCherry was bleached (compare top row, pre- and postbleach images, white arrows), but there was no visible increase in intensity of the GFP-Rem fluorescence (Fig. 4C, compare bottom row, pre- and postbleach images, yellow arrows), and the AP-FRET efficiency between the two proteins was only 7.9% ± 5.7% (Fig. 4D). As additional controls, mCherry alone did not demonstrate efficient FRET with FITC-labeled Gag in NMuMG-C3H cells (10.7% ± 6.5%), and the background level of AP-FRET between mCherry and GFP was 3.9% ± 1.2% (Fig. 4D), indicating that the high level of AP-FRET between FITC-labeled Gag and RPL9-mCherry was specific for Gag and L9. Taken together, the results of these experiments indicate that Gag and L9 form a com-

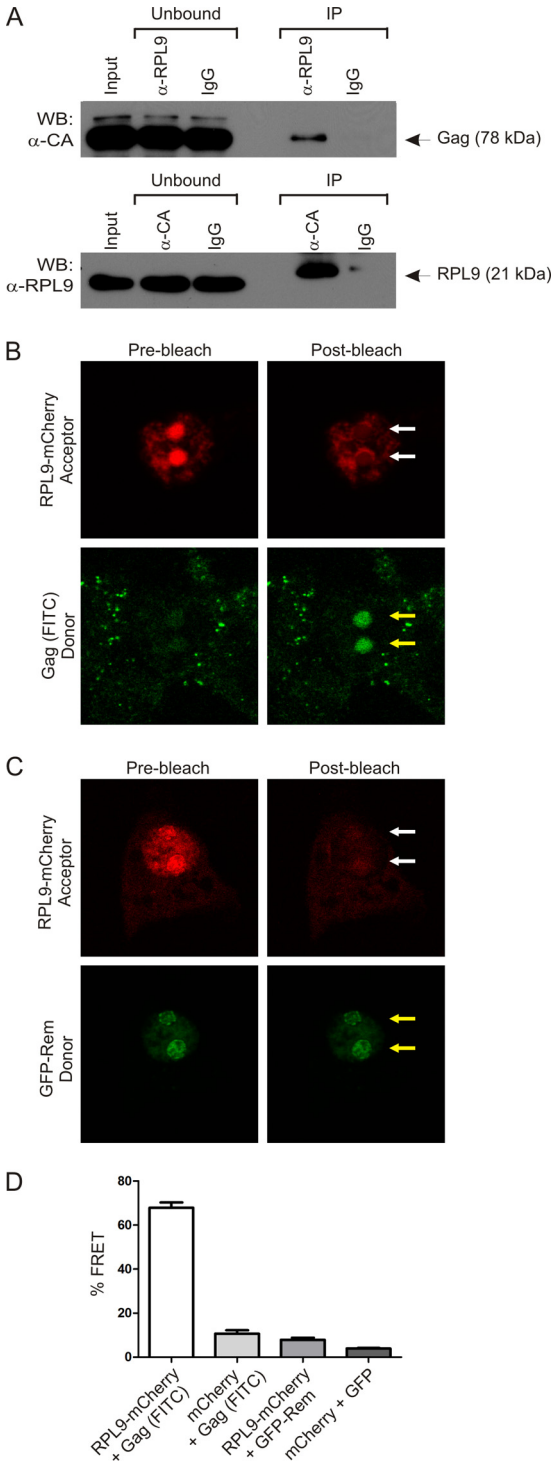

FIG 4 MMTV Gag interacts with L9 in nucleoli. (A) RPL9 (top) or MMTV Gag (bottom) was immunoprecipitated from NMuMG-C3H cell lysates using anti-L9 or anti-CA antibodies, respectively, and anti-lamin antibody isotype control (IgG) was used to show specificity. Proteins present in the input, unbound, or coimmunoprecipitated (IP) fractions were analyzed by Western blotting (WB) using anti-CA/Gag (top) or anti-RPL9 (bottom) antibodies. The arrows point to the bands corresponding to Gag (~78 kDa) (top) and L9 (~21 kDa) (bottom). (B) AP-FRET analysis of RPL9-mCherry (acceptor) and MMTV Gag-FITC (donor) in MMTV(C3H)-infected NMuMG cells. The confocal images represent raw data used for FRET analysis. Prebleach images were acquired and are shown on the left. Postbleach images were obtained after bleaching the nucleus with a 543-nm laser to remove most of the RPL9-mCherry fluorescent signal (white arrows). MMTV Gag was detected by immunofluorescence using anti-CA primary antibody and FITC-labeled secondary antibody, with prebleach and postbleach images shown. The yellow arrows point to the dramatic increase in fluorescence signal of Gag-FITC in nucleoli due to dequenching following bleaching of RPL9-mCherry. (C) GFP-Rem and RPL9-mCherry coexpressed in NMuMG cells. Confocal microscopy images were obtained as for panel B. The white arrows indicate bleaching of the RPL9-mCherry acceptor fluorophore, and the yellow arrows point to the signal for GFP-Rem, which is not noticeably changed. (D) Comparison of AP-FRET efficiency values obtained from the following protein pairs: RPL9-mCherry and viral C3H Gag (FITC stained), mCherry alone and viral C3H Gag (FITC stained), RPL9-mCherry and MMTV GFP-Rem, and mCherry and GFP expression vectors. The error bars indicate standard error of the mean.

plex in nucleoli, likely through a direct protein-protein interaction.

The CA domain is the major determinant of Gag-L9 interaction. We next sought to identify the region of Gag that interacts with L9. Single domains of MMTV Gag or Gag truncation mutants tagged with GFP (Fig. 5A) were expressed in uninfected NMuMG cells with or without RPL9-mCherry. When expressed alone, MMTV NC-GFP was nucleolar, as determined by the identification of nucleoli in the difference interference contrast (DIC) microscopy images (Fig. 5B, yellow arrow). In contrast, when NC was deleted from Gag (MA-CA.GFP), the truncated protein was predominantly cytoplasmic, with faint nuclear fluorescence that excluded nucleoli (Fig. 5C, top). However, when coexpressed with RPL9-mCherry, MA-CA.GFP localized exclusively to nucleoli (Fig. 5D, top row). Quantitation of the representative images in the top row of Fig. 5D using Mander's analysis revealed that 100% of the MA-CA.GFP protein colocalized with L9 (M_1), and reciprocally, 86% of the L9 signal overlapped with MA-CA.GFP (M_2).

To determine whether the CA region was sufficient to mediate the interaction between Gag and L9, the subcellular distribution of CA-GFP was tested in the absence or presence of L9 overexpression. CA-GFP was diffuse throughout the cell, with nucleolar exclusion when expressed alone (Fig. 5C, middle). However, coexpression with RPL9-mCherry resulted in a striking relocalization of CA-GFP to nucleoli and complete colocalization with L9 (Mander's analysis; $M_1 = 100\%$; $M_2 = 93\%$) (Fig. 5D, middle row). In contrast, expression of RPL9-mCherry had no effect on the distribution of GFP alone (Fig. 5C, bottom). These results indicate that the major determinant of the Gag-L9 interaction maps to the CA region, although other regions may play contributing roles.

Gag-L9 interaction is conserved in lower eukaryotes. To gain insight into the region(s) of L9 that interacts with MMTV Gag, we compared the amino acid sequence of murine L9 to those of several other eukaryotic species (Table 1). L9 was highly conserved among vertebrates, with the murine amino acid sequence bearing high homology and identity to human (99% homology; 98% identity), rat (99% homology; 98% identity), chicken (98% homology; 94% identity), and zebrafish (95% homology; 89% identity) sequences. As expected, there was less sequence conservation between murine and *D. melanogaster* L9 (80% homology; 64% identity). Interestingly, two isoforms of L9 have been reported in yeast, differing by only 3 amino acids (41, 42). Murine L9 was 69% homologous and 49% identical to yeast L9A and 69% homologous and 50% identical to yeast L9B (Fig. 6A). To test whether yeast L9 would also relocalize MMTV Gag, we expressed

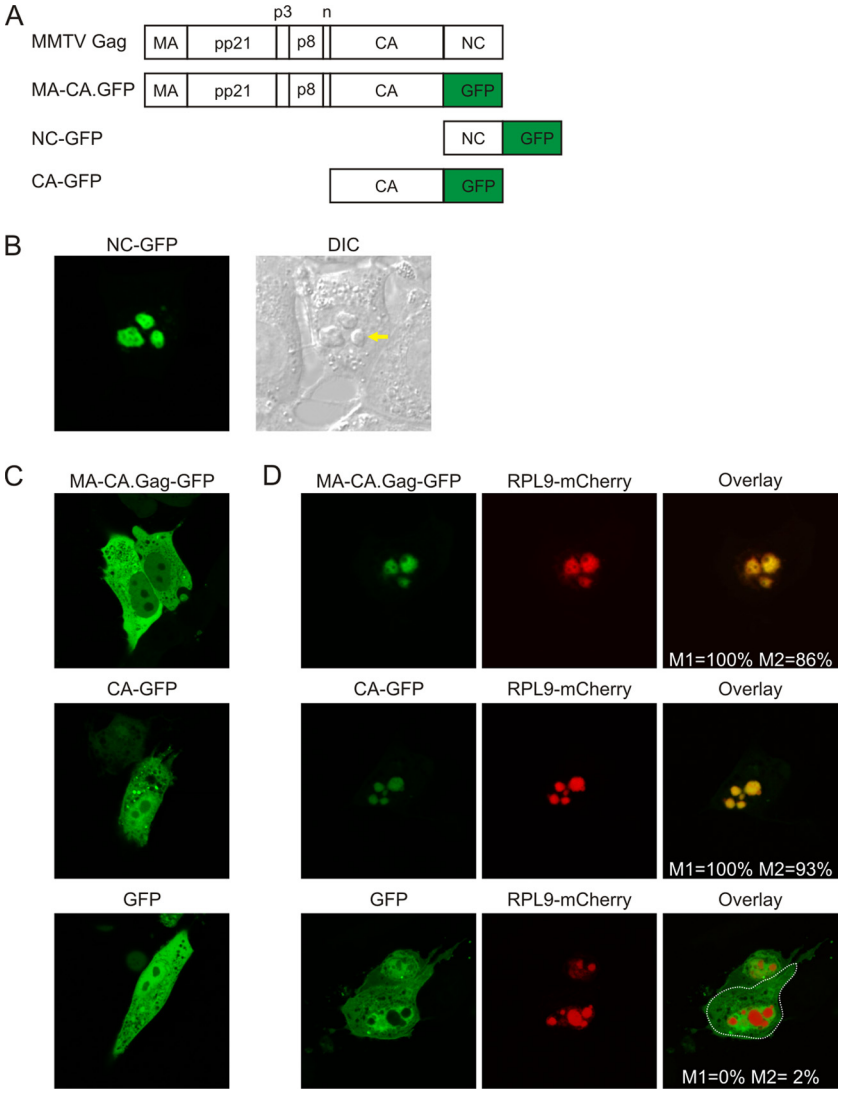

FIG 5 L9 interacts with the CA domain of MMTV Gag. (A) GFP-tagged MMTV Gag deletion constructs. (B) Confocal microscopy image of GFP-tagged MMTV NC expressed in NMuMG, with the yellow arrow pointing to a nucleolus. (C) Confocal microscopy images of Gag-GFP deletion mutants expressed alone in NMuMG cells. (D) Confocal microscopy images of Gag-GFP deletion mutants coexpressed with RPL9-mCherry in NMuMG cells. M_1 and M_2 colocalization values for single cells (top and middle) or the cell outlined with a white dotted line (bottom) were determined using ImageJ JACoP.

mCherry-tagged yeast L9B in NMuMG-C3H cells. Interestingly, yeast L9B localized to nucleoli in murine cells, suggesting that its nucleolar localization signal (NoLS) remained functional, and it induced Gag to accumulate in nucleoli (Fig. 6B). This result indicates that the region of L9 that interacts with MMTV Gag resides in the portion of the protein that is conserved between murine and yeast L9.

TABLE 1 Amino acid comparison to mouse RPL9 (NCBI NM_011292)

Species	Homology (%)	Identity (%)	Accession no.
Human	99	98	NM_001024921
Rat	99	98	NM_001007598
Chicken	98	94	XM_423225
Zebrafish	95	89	NM_001003861
Fruit fly	80	64	NM_057813
Yeast A	69	49	NP_011368
Yeast B	69	50	NP_014332

Gag interacts with the C-terminal region of L9. Sequence comparison between the mouse and yeast L9 proteins revealed the highest level of conservation within the C-terminal region of L9 (Fig. 6A; the red vertical line denotes the junction of N- and C-terminal domains). To determine whether the C-terminal region of L9 was sufficient to interact with Gag, we coexpressed mCherry-tagged N- or C-terminal fragments of L9 (Fig. 7A) with Gag-GFP in NMuMG cells. The N-terminal fragment of L9 (RPL9.NT-mCh) localized to nucleoli of NMuMG cells. However, Gag-GFP did not accumulate within nucleoli of cells expressing the N-terminal fragment (Fig. 7B, top row). In contrast, the C-terminal fragment of L9 (RPL9.CT-mCh) accumulated in small cytoplasmic foci that partially colocalized with Gag-GFP (Manders analysis; $M_1 = 36\%$; $M_2 = 25\%$) (Fig. 7B, bottom row). No colocalization was seen in MMTV-infected NMuMG-C3H cells between Gag and RPL9.NT-mCh (Fig. 7C, top row), and again, partial colocalization was observed between the C-terminal region of L9

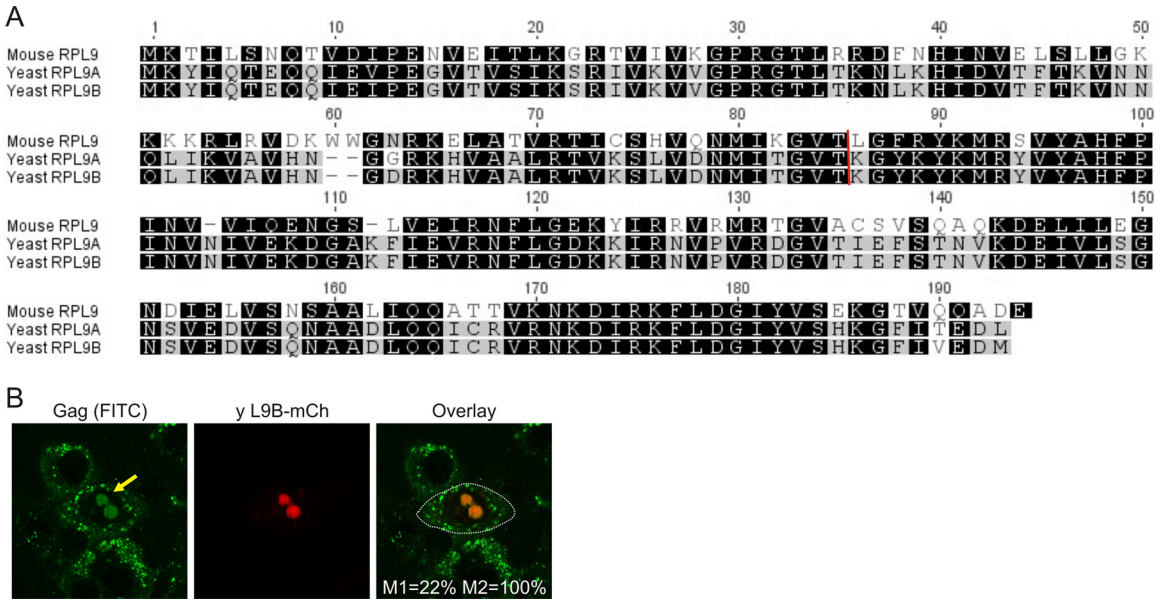

FIG 6 The Gag-L9 interaction is conserved in lower eukaryotes. (A) Protein sequence alignments between mouse RPL9, *S. cerevisiae* RPL9A, and *S. cerevisiae* RPL9B. The vertical red line indicates the dividing line between the N-terminal and C-terminal domains. Black shading indicates residues that are homologous among all of the sequences, and gray shading highlights homologous residues present in at least two of the sequences. Alignments were constructed using BLOSUM62 in Geneious v. 5.5.6. (B) Confocal microscopy images of *S. cerevisiae* RPL9B-mCherry expressed in NMuMG-C3H cells fixed and immunostained for Gag. The yellow arrow points to the presence of Gag in nucleoli. M_1 and M_2 colocalization values for the cell outlined with a white dotted line (bottom) were determined using ImageJ JACoP.

and Gag in cells expressing RPL9.CT-mCh (M_1 = 15%; M_2 = 18%) (Fig. 7C, bottom row). These data suggest that the NoLS for L9 is in the N-terminal half of the protein, whereas the C-terminal portion may contain the Gag interaction domain.

To test whether the C terminus of L9 was sufficient to relocalize Gag to nucleoli, we fused a heterologous NoLS from the HIV-1 Rev protein onto the L9 C-terminal domain in an attempt to restore proper localization of L9 (Fig. 7D). First, we demonstrated that the Rev NoLS would drive mCherry into the nucleolus (Rev.NoLS-mCherry) (Fig. 7E, top row, middle image). However, this nucleolar protein was not capable of relocalizing Gag-GFP (Fig. 7E, top row, left image). In contrast, when Gag-GFP was coexpressed with the C-terminal fragment of L9 fused to the Rev.NoLS (RPL9.CT.Rev-mCherry), Gag-GFP was relocalized to nucleoli and partially colocalized with the L9 chimeric protein in nucleoli (Fig. 7E, bottom row, yellow arrow) (M_1 = 4%; M_2 = 92%). Thus, the C-terminal domain of L9 was sufficient for relocalization of Gag, provided that L9 contains a functional NoLS. Interestingly, deleting the C-terminal 26 amino acids, which contain the highest degree of conservation between mouse and yeast L9B (Fig. 6A), from L9 did not disrupt the Gag-L9 interaction, indicating that this sequence is not required for Gag to interact with L9 (data not shown).

Knockdown of L9 expression interferes with MMTV production. Finding that L9 and Gag interacted in the nucleolus raised the possibility that L9 could play a role in virus production. To test this idea, we used a pool of three L9-specific siRNAs to reduce L9 expression by approximately 35% compared to scrambled control siRNA ($P < 0.05$) (Fig. 8A), relative to GAPDH, the internal control. The modest L9 knockdown likely results from long-lived L9 present in ribosomes, which are turned over as a functional unit with a half-life of 96 to 120 h (43, 44), and therefore would be largely unaffected by the transient knockdown. Indeed, when we examined the L9 distribution in siRNA-treated cells by immunofluorescence, we observed no difference in the distribution or the amount of cytoplasmic L9 (Fig. 8B). However, in L9-specific siRNA-transfected cells, L9 was not detected in nucleoli, indicating that the knockdown primarily affected the extraribosomal pool of L9 prior to its incorporation into ribosomes. Furthermore, the siRNA-treated cells maintained normal morphology, suggesting that the L9 knockdown was not overtly toxic, and the cytoplasmic distribution of Gag was not obviously altered (Fig. 8B). Because L9 is essential for ribosomal function, we next tested whether this degree of L9 knockdown affected steady-state levels of Gag. We found that L9 knockdown did not result in a significant decrease in Gag expression relative to GAPDH loading controls (Fig. 8C). However, the virus yield from cells treated with L9 siRNA was reduced by ~50% relative to the scrambled siRNA control ($P < 0.005$) (Fig. 8D) when normalized to intracellular Gag levels. This finding suggests that the Gag-L9 interaction is intrinsic to the virus assembly and budding pathway, although we cannot rule out the possibility that the defect in virus production is due to an indirect effect of the L9 siRNA treatment.

DISCUSSION

Retrovirus-cell interactions that contribute to the processes of virus assembly and budding remain incompletely understood. In particular, the functions of host factors that engage retroviral Gag proteins far from the site of virus budding are difficult to unravel. In this work, we report the novel finding that L9, a protein that resides in the nucleolus prior to its incorporation into ribosomes, interacts with the MMTV Gag protein and influences virus assembly. This report is the first to find an interaction between Gag and

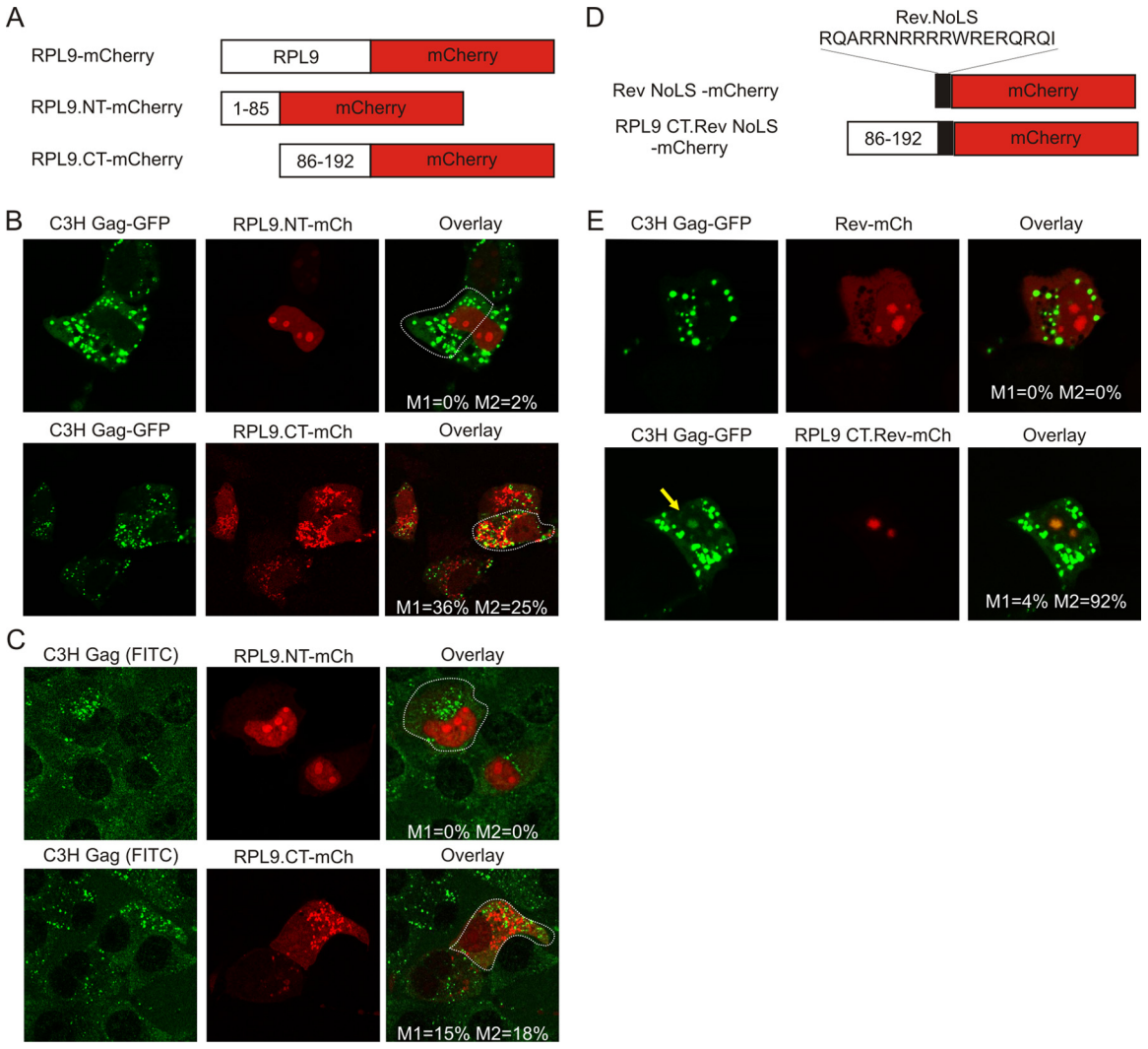

FIG 7 Mapping the Gag interaction domain within L9. (A) Schematic of the N-terminal and C-terminal regions of RPL9 fused to mCherry. RPL9.NT consists of RPL9 amino acids 1 to 85, and RPL9.CT consists of amino acids 86 to 192. (B) Confocal microscopy of NMuMG cells cotransfected with MMTV(C3H) Gag-GFP and mCherry-fused RPL9 N- or C-terminal domains. (C) Confocal microscopy of MMTV(C3H)-infected NMuMG cells transfected with the N- or C-terminal RPL9-mCherry construct. Gag was detected with anti-CA primary antibody and FITC-conjugated secondary antibody. (D) Schematic diagram of the HIV-1 Rev NoLS fused to the N terminus of mCherry and inserted into the RPL9.CT-mCherry construct between the RPL9 and mCherry sequences. (E) Confocal images of Gag-GFP coexpressed with Rev NoLS-containing constructs. The yellow arrow indicates the presence of Gag in the nucleolus with coexpression of RPL9 CT.Rev-mCh. For each of the overlay images, M_1 and M_2 colocalization values for single cells or those outlined with white dots were calculated using ImageJ JACoP.

a ribosomal protein. We propose that virus assembly may be modulated by this interaction.

Why is the MMTV Gag protein present in the nucleolus in association with L9, a constituent of the large preribosome complex? These data raise the intriguing possibility that L9 has an extraribosomal function, possibly one that contributes to Gag-mediated virus assembly. Recently, overexpression of ribosomal protein L4 was found to increase readthrough of the murine leukemia virus (MLV) pseudoknot, which is required to produce the MLV Gag-Pol fusion protein (45). This imbalance in the Gag/Gag-Pol ratio led to an assembly defect, possibly due to steric constraints imposed by excess Gag-Pol on virus particle assembly. MMTV uses ribosomal frameshifting rather than readthrough to produce Gag-Pro and Gag-Pro-Pol fusion proteins (46). In our experiments, we did not detect a change in the Gag/Gag-Pol ratio by Western blotting following L9 knockdown, suggesting that the reduction in particle production we observed was unlikely to be due to a change in the efficiency of frameshifting.

It is not evident from our data whether the effect of L9 on virus assembly is directly related to an extraribosomal activity of L9 or whether another host factor is recruited into the Gag-L9 complex. The influence of L9 appears to occur early in the assembly pathway, as we have no evidence that L9 colocalizes with Gag at cytoplasmic sites of capsid assembly, nor have we detected L9 in virus particles (data not shown). Moreover, because Gag and L9 associated in the nucleolus, other nucleolar proteins or RNAs may contribute to virus assembly. Candidates include nucleolin and B23, which modulate HIV-1 assembly (47–52), and small nuclear RNAs, products of Pol III transcription at the nucleolar periphery, which are selectively incorporated in retrovirus particles (53–57).

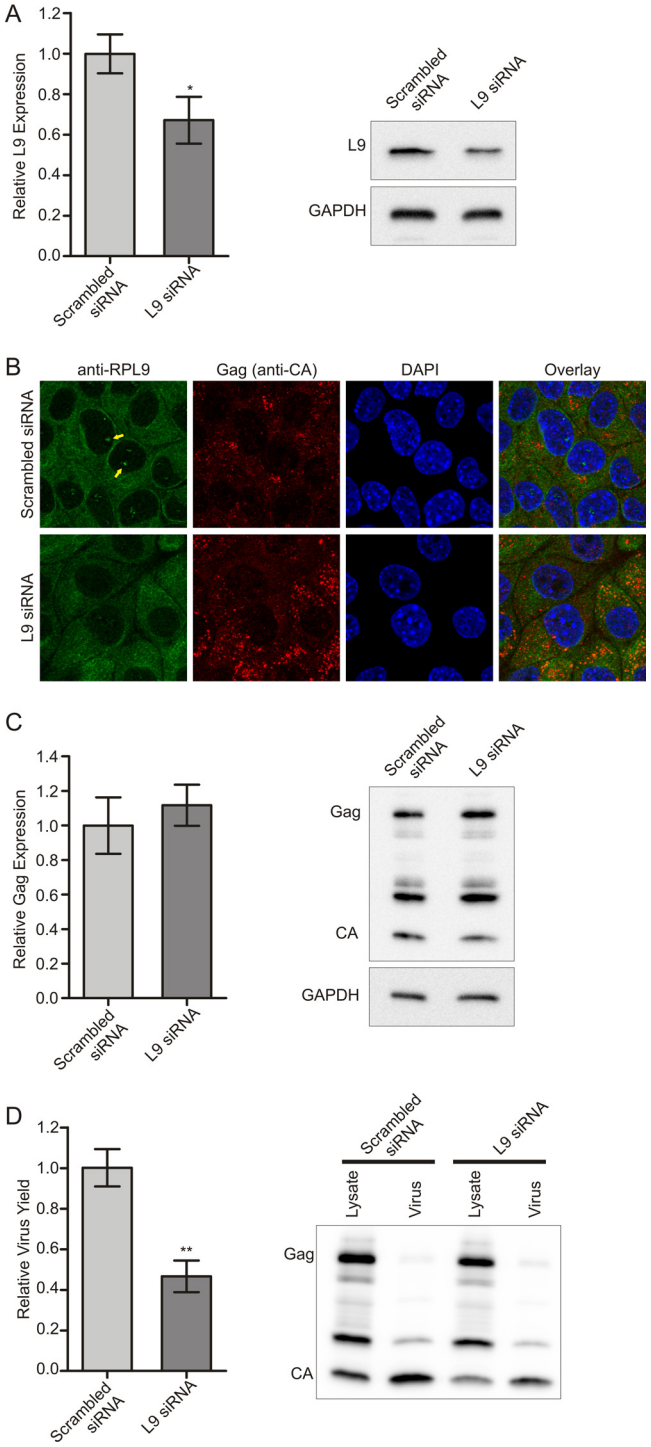

FIG 8 Effect of L9 depletion on MMTV virus yield. MMTV-infected NMuMG-C3H cells were treated with L9-specific or scrambled control siRNAs. (A) Effect of L9-siRNA treatment on L9 expression relative to GAPDH loading controls, with the error bars representing the mean ± standard error of the mean ($n = 7$). A two-tailed Student's t test was performed to compare the treatment groups; *, $P < 0.05$. A representative Western blot is shown on the right of the graph, demonstrating selective reduction in L9 expression. (B) Cells treated with L9-specific or control siRNAs were immunostained for L9 and imaged using fluorescence confocal microscopy. The yellow arrows in the scrambled siRNA images point to L9 immunofluorescence in nucleoli, which is absent from the L9-siRNA-treated cells below. (C and D) The samples from panel A were used to evaluate steady-state Gag levels (C) and virus yield (D) relative to scrambled siRNA treatment and normalized for GAPDH expression levels. The virus yield was calculated as the amount of Gag in the sucrose-purified media divided by the sum of Gag in the lysates and media. Representative Western blots from each experiment are shown on the right of the graphs. The graphs show means ± standard errors of the mean; **, $P < 0.005$.

Future experiments will explore whether modulating L9 expression levels alters MMTV infectivity, incorporation of viral genomic RNA, or enrichment of Pol III-transcribed cellular RNAs into virions.

Localization of MMTV Gag to the nucleus or nucleolus has not been reported previously, although other retroviral Gag proteins do traffic transiently through the nucleus (references 58–65; reviewed in reference 66). For RSV, genetic and biochemical evidence suggests that genomic RNA packaging is linked to nuclear trafficking of Gag (33, 65, 67), but whether this role is conserved for other retroviruses is not known. What is the mechanism of MMTV Gag nucleolar localization? Finding that the MMTV NC protein contains nucleolar localization activity suggests that it may contain the Gag NoLS. In addition, our data clearly showed that increasing the intracellular level of L9 induced the accumulation of Gag in nucleoli through an interaction with the CA region. Thus, it is feasible that the degree of MMTV Gag nucleolar localization varies due to cell type differences in L9 or other factors. It is also possible that Gag-L9 interactions are initiated in the cytoplasm and Gag piggybacks into the nucleolus with L9. Further experiments will be needed to differentiate between these possibilities.

Interestingly, many ribosomal proteins have well-established extraribosomal functions mediated by their RNA binding properties and protein-protein interaction domains. For example, several ribosomal proteins autoregulate their synthesis by altering splicing or translation of their own mRNA (reviewed in reference 68). Furthermore, L26 binds to the 5′ UTR of p53 mRNA, stimulating p53 translation (69), and extraribosomal L11 modulates levels of c-myc by recruiting microRNA (miRNA) and a component of the RNA-induced silencing complex to the 3′ UTR of the c-myc gene (70) in response to nucleolar stress. Other ribosomal proteins engage in protein-protein interactions that modulate cellular functions, including those that serve as sentinels to identify states of cellular stress triggered by ribosomal dysfunction. Specifically, ribosomal proteins L5, L11, L23, and S7 activate p53 by binding to MDM2, resulting in cell cycle arrest or apoptosis (71–74). L23 sequesters nucleophosmin in the nucleolus, preventing it from interacting with a c-myc antagonist, leading to stimulated cell growth (75). Ribosomal protein S3 can be induced to undergo nuclear import, where it binds to NF-κB to stimulate gene-specific transcription (76). As further evidence of their critical extraribosomal functions, mutations in ribosomal proteins are associated with the human diseases Diamond-Blackfan anemia and 5q syndrome, and dysregulated ribosomal protein expression occurs in cancers, such as hepatocellular, colorectal, and prostate cancer and melanoma, sarcoma, and lymphoma (77, 78). L9 and other ribosomal proteins act as tumor suppressors, consistent with observations that mutations in genes encoding ribosomal proteins lead to malignant diseases (12, 79–82).

Because ribosomal proteins are present in all cells and play a central role in modulating cell cycle arrest, proliferation, transcription, translation, DNA repair, and stress responses, it has

been suggested that they are prime targets of viruses, which commonly hijack host machinery to facilitate their own replication (68). Accordingly, it is not surprising that diverse families of viruses have been reported to interact with ribosomal proteins. During hepatitis C virus (HCV) infection, S5 and S9 interact with the internal ribosome entry site (IRES) on the HCV RNA to position the IRES on the 40S ribosomal subunit for optimal translation of viral proteins (83). The noncoding EBER-1 RNA of Epstein-Barr virus (EBV) binds to and relocalizes L22, although the biological relevance of this finding in EBV infection is not known (84, 85). Among retroviruses, infection with RSV or Abelson murine leukemia virus (Ab-MuLV) results in phosphorylation of S6 (86, 87). The role of S6 phosphorylation in retrovirus infection is unclear, but data from cells transformed with simian virus 40 (SV40) suggest that S6 phosphorylation may promote cell growth and oncogenic transformation (88). Recently, it was shown that L4 modulates Moloney murine leukemia virus translational readthrough, which is required for maintenance of the proper Gag/Gag-Pol ratio (45). Up to now, no other retroviral proteins have been reported to interact with ribosomal proteins either within ribosomal subunits or in an extraribosomal setting.

Interestingly, two other MMTV-encoded proteins, the Rem nuclear export factor (5) and the signal peptide of Rem and Env, known as p14 (89), independently localize to nucleoli in infected cells. Therefore, it is plausible that Gag, Rem, and/or p14 encounter one another within nucleoli. The p14 protein was recently found to regulate transcription levels of ribosomal protein L5, which interferes with MDM2-mediated degradation of p53 (7, 90). In addition, the MMTV Env protein transforms mammary cells in culture (7), and enhanced tumorigenicity *in vivo* maps to the *gag* gene (6). Thus, the mechanism by which MMTV induces tumors in mice appears to be more complex than previously realized. The newly appreciated role of the nucleolus and the ribosomal proteins that interact with MMTV proteins opens the door to advancing our understanding of how viruses intersect with host regulatory pathways to replicate and cause disease.

ACKNOWLEDGMENTS

We thank Anita Hopper, Ohio State University; Bryan Cullen, Duke University; Jackie Dudley, University of Texas at Austin; Tim Krüger, University of Würzburg, Würzburg, Germany; Mark Olson, University of Mississippi Medical Center; Susan Ross, University of Pennsylvania; and Roger Tsien, University of California at San Diego, for their contributions of reagents and materials used in this study and members of the Parent Laboratory (E. Ryan and T. Lochmann) for plasmid construction. We also acknowledge the Penn State College of Medicine Molecular Genetics and Imaging Core Facilities for DNA sequencing and confocal microscopy imaging.

We greatly appreciate support from the NIH (grants R01 CA76534 to L.J.P., F30 CA165774 to D.V.B., R01 CA113784 to T.V.G., and R01 CA30488 to S.P.G.), the NSF (Graduate Research Fellowship to A.R.B.), and the Pennsylvania Department of Health Tobacco Settlement Funds (Graduate Research Supplement Award to A.R.B. and L.J.P.).

The Pennsylvania Department of Health specifically disclaims responsibility for any analyses, interpretations, or conclusions of this project.

REFERENCES

1. **Bittner JJ.** 1936. Some possible effects of nursing on the mammary gland tumor incidence in mice. Science **84**:162.
2. **Bergman AC, Bjornberg O, Nord J, Nyman PO, Rosengren AM.** 1994. The protein p30, encoded at the gag-pro junction of mouse mammary tumor virus, is a dUTPase fused with a nucleocapsid protein. Virology **204**:420–424.
3. **Choi Y, Kappler JW, Marrack P.** 1991. A superantigen encoded in the open reading frame of the 3′ long terminal repeat of mouse mammary tumour virus. Nature **350**:203–207.
4. **Indik S, Gunzburg WH, Salmons B, Rouault F.** 2005. A novel, mouse mammary tumor virus encoded protein with Rev-like properties. Virology **337**:1–6.
5. **Mertz JA, Simper MS, Lozano MM, Payne SM, Dudley JP.** 2005. Mouse mammary tumor virus encodes a self-regulatory RNA export protein and is a complex retrovirus. J. Virol. **79**:14737–14747.
6. **Hook LM, Agafonova Y, Ross SR, Turner SJ, Golovkina TV.** 2000. Genetics of mouse mammary tumor virus-induced mammary tumors: linkage of tumor induction to the gag gene. J. Virol. **74**:8876–8883.
7. **Katz E, Lareef MH, Rassa JC, Grande SM, King LB, Russo J, Ross SR, Monroe JG.** 2005. MMTV Env encodes an ITAM responsible for transformation of mammary epithelial cells in three-dimensional culture. J. Exp. Med. **201**:431–439.
8. **Chandramouli P, Topf M, Menetret JF, Eswar N, Cannone JJ, Gutell RR, Sali A, Akey CW.** 2008. Structure of the mammalian 80S ribosome at 8.7 A resolution. Structure **16**:535–548.
9. **Suzuki K, Olvera J, Wool IG.** 1990. The primary structure of rat ribosomal protein L9. Gene **93**:297–300.
10. **Wool IG, Chan YL, Gluck A.** 1995. Structure and evolution of mammalian ribosomal proteins. Biochem. Cell Biol. **73**:933–947.
11. **Schmidt A, Hollmann M, Schafer U.** 1996. A newly identified Minute locus, M(2)32D, encodes the ribosomal protein L9 in Drosophila melanogaster. Mol. Gen. Genet. **251**:381–387.
12. **MacInnes AW, Amsterdam A, Whittaker CA, Hopkins N, Lees JA.** 2008. Loss of p53 synthesis in zebrafish tumors with ribosomal protein gene mutations. Proc. Natl. Acad. Sci. U. S. A. **105**:10408–10413.
13. **Golden BL, Ramakrishnan V, White SW.** 1993. Ribosomal protein L6: structural evidence of gene duplication from a primitive RNA binding protein. EMBO J. **12**:4901–4908.
14. **Marion MJ, Marion C.** 1987. Localization of ribosomal proteins on the surface of mammalian 60S ribosomal subunits by means of immobilized enzymes. Correlation with chemical cross-linking data. Biochem. Biophys. Res. Commun. **149**:1077–1083.
15. **Montanaro L, Trere D, Derenzini M.** 2008. Nucleolus, ribosomes, and cancer. Am. J. Pathol. **173**:301–310.
16. **Olson MO, Dundr M.** 2005. The moving parts of the nucleolus. Histochem. Cell Biol. **123**:203–216.
17. **Kruger T, Zentgraf H, Scheer U.** 2007. Intranucleolar sites of ribosome biogenesis defined by the localization of early binding ribosomal proteins. J. Cell Biol. **177**:573–578.
18. **Callahan EM, Wills JW.** 2000. Repositioning basic residues in the M domain of the Rous sarcoma virus gag protein. J. Virol. **74**:11222–11229.
19. **Dundr M, Misteli T, Olson MO.** 2000. The dynamics of postmitotic reassembly of the nucleolus. J. Cell Biol. **150**:433–446.
20. **Shaner NC, Campbell RE, Steinbach PA, Giepmans BN, Palmer AE, Tsien RY.** 2004. Improved monomeric red, orange and yellow fluorescent proteins derived from Discosoma sp. red fluorescent protein. Nat. Biotechnol. **22**:1567–1572.
21. **Cochrane AW, Perkins A, Rosen CA.** 1990. Identification of sequences important in the nucleolar localization of human immunodeficiency virus Rev: relevance of nucleolar localization to function. J. Virol. **64**:881–885.
22. **Malim MH, Bohnlein S, Hauber J, Cullen BR.** 1989. Functional dissection of the HIV-1 Rev trans-activator: derivation of a trans-dominant repressor of Rev function. Cell **58**:205–214.
23. **Malim MH, Hauber J, Fenrick R, Cullen BR.** 1988. Immunodeficiency virus rev trans-activator modulates the expression of the viral regulatory genes. Nature **335**:181–183.
24. **Luban J, Bossolt KL, Franke EK, Kalpana GV, Goff SP.** 1993. Human immunodeficiency virus type 1 Gag protein binds to cyclophilins A and B. Cell **73**:1067–1078.
25. **Tachedjian G, Goff SP.** 2003. The effect of NNRTIs on HIV reverse transcriptase dimerization. Curr. Opin. Investig. Drugs **4**:966–973.
26. **Dzuris JL, Golovkina TV, Ross SR.** 1997. Both T and B cells shed infectious mouse mammary tumor virus. J. Virol. **71**:6044–6048.
27. **Jude BA, Pobezinskaya Y, Bishop J, Parke S, Medzhitov RM, Chervonsky AV, Golovkina TV.** 2003. Subversion of the innate immune system by a retrovirus. Nat. Immunol. **4**:573–578.
28. **Owens RB, Hackett AJ.** 1972. Tissue culture studies of mouse mammary tumor cells and associated viruses. J. Natl. Cancer Inst. **49**:1321–1332.
29. **Craven RC, Leure-duPree AE, Weldon RA, Jr, Wills JW.** 1995. Genetic

analysis of the major homology region of the Rous sarcoma virus Gag protein. J. Virol. **69**:4213–4227.
30. **Purdy A, Case L, Duvall M, Overstrom-Coleman M, Monnier N, Chervonsky A, Golovkina T.** 2003. Unique resistance of I/LnJ mice to a retrovirus is due to sustained interferon gamma-dependent production of virus-neutralizing antibodies. J. Exp. Med. **197**:233–243.
31. **Abramoff MD, Magalhaes PJ, Ram SJ.** 2004. Image processing with ImageJ. Biophotonics Int. **11**:36–42.
32. **Bolte S, Cordelieres FP.** 2006. A guided tour into subcellular colocalization analysis in light microscopy. J. Microsc. **224**:213–232.
33. **Kenney SP, Lochmann TL, Schmid CL, Parent LJ.** 2008. Intermolecular interactions between retroviral Gag proteins in the nucleus. J. Virol. **82**: 683–691.
34. **Swanson I, Jude BA, Zhang AR, Pucker A, Smith ZE, Golovkina TV.** 2006. Sequences within the gag gene of mouse mammary tumor virus needed for mammary gland cell transformation. J. Virol. **80**:3215–3224.
35. **Ban N, Nissen P, Hansen J, Moore PB, Steitz TA.** 2000. The complete atomic structure of the large ribosomal subunit at 2.4 A resolution. Science **289**:905–920.
36. **Taylor DJ, Devkota B, Huang AD, Topf M, Narayanan E, Sali A, Harvey SC, Frank J.** 2009. Comprehensive molecular structure of the eukaryotic ribosome. Structure **17**:1591–1604.
37. **Garber ED, Hauth FC.** 1950. A new mutation with asymmetrical expression in the mouse. J. Heredity **41**:122–124.
38. **Owens RB.** 1974. Glandular epithelial cells from mice: a method for selective cultivation. J. Natl. Cancer Inst. **52**:1375–1378.
39. **Owens RB, Smith HS, Hackett AJ.** 1974. Epithelial cell cultures from normal glandular tissue of mice. J. Natl. Cancer Inst. **53**:261–269.
40. **Albertazzi L, Arosio D, Marchetti L, Ricci F, Beltram F.** 2009. Quantitative FRET analysis with the EGFP-mCherry fluorescent protein pair. Photochem. Photobiol. **85**:287–297.
41. **Gudipati RK, Neil H, Feuerbach F, Malabat C, Jacquier A.** 2012. The yeast RPL9B gene is regulated by modulation between two modes of transcription termination. EMBO J. **31**:2427–2437.
42. **Jones DG, Reusser U, Braus GH.** 1991. Cloning and characterisation of a yeast homolog of the mammalian ribosomal protein L9. Nucleic Acids Res. **19**:5785.
43. **Hirsch CA, Hiatt HH.** 1966. Turnover of liver ribosomes in fed and in fasted rats. J. Biol. Chem. **241**:5936–5940.
44. **Retz KC, Steele WJ.** 1980. Ribosome turnover in rat brain and liver. Life Sci. **27**:2601–2604.
45. **Green L, Houck-Loomis B, Yueh A, Goff SP.** 2012. Large ribosomal protein 4 increases efficiency of viral recoding sequences. J. Virol. **86**: 8949–8958.
46. **Jacks T, Townsley K, Varmus HE, Majors J.** 1987. Two efficient ribosomal frameshifting events are required for synthesis of mouse mammary tumor virus gag-related polyproteins. Proc. Natl. Acad. Sci. U. S. A. **84**: 4298–4302.
47. **Bacharach E, Gonsky J, Alin K, Orlova M, Goff SP.** 2000. The carboxy-terminal fragment of nucleolin interacts with the nucleocapsid domain of retroviral gag proteins and inhibits virion assembly. J. Virol. **74**:11027–11039.
48. **Fankhauser C, Izaurralde E, Adachi Y, Wingfield P, Laemmli UK.** 1991. Specific complex of human immunodeficiency virus type 1 rev and nucleolar B23 proteins: dissociation by the rev response element. Mol. Cell. Biol. **11**:2567–2575.
49. **Miyazaki Y, Nosaka T, Hatanaka M.** 1996. The post-transcriptional regulator Rev of HIV: implications for its interaction with the nucleolar protein B23. Biochimie **78**:1081–1086.
50. **Miyazaki Y, Takamatsu T, Nosaka T, Fujita S, Martin TE, Hatanaka M.** 1995. The cytotoxicity of human immunodeficiency virus type 1 Rev: implications for its interaction with the nucleolar protein B23. Exp. Cell Res. **219**:93–101.
51. **Szebeni A, Mehrotra B, Baumann A, Adam SA, Wingfield PT, Olson MO.** 1997. Nucleolar protein B23 stimulates nuclear import of the HIV-1 Rev protein and NLS-conjugated albumin. Biochemistry **36**:3941–3949.
52. **Ueno T, Tokunaga K, Sawa H, Maeda M, Chiba J, Kojima A, Hasegawa H, Shoya Y, Sata T, Kurata T, Takahashi H.** 2004. Nucleolin and the packaging signal, psi, promote the budding of human immunodeficiency virus type-1 (HIV-1). Microbiol. Immunol. **48**:111–118.
53. **Garcia EL, Onafuwa-Nuga A, Sim S, King SR, Wolin SL, Telesnitsky A.** 2009. Packaging of host mY RNAs by murine leukemia virus may occur early in Y RNA biogenesis. J. Virol. **83**:12526–12534.
54. **Keene SE, King SR, Telesnitsky A.** 2010. 7SL RNA is retained in HIV-1 minimal virus-like particles as an S-domain fragment. J. Virol. **84**:9070–9077.
55. **Keene SE, Telesnitsky A.** 2012. *cis*-Acting determinants of 7SL RNA packaging by HIV-1. J. Virol. **86**:7934–7942.
56. **Onafuwa-Nuga AA, Telesnitsky A, King SR.** 2006. 7SL RNA, but not the 54-kd signal recognition particle protein, is an abundant component of both infectious HIV-1 and minimal virus-like particles. RNA **12**:542–546.
57. **Rulli SJ, Jr, Hibbert CS, Mirro J, Pederson T, Biswal S, Rein A.** 2007. Selective and nonselective packaging of cellular RNAs in retrovirus particles. J. Virol. **81**:6623–6631.
58. **Bohl C, Brown S, Weldon R, Jr.** 2005. The pp24 phosphoprotein of Mason-Pfizer monkey virus contributes to viral genome packaging. Retrovirology **2**:68.
59. **Dupont S, Sharova N, DeHoratius C, Virbasius CM, Zhu X, Bukrinskaya AG, Stevenson M, Green MR.** 1999. A novel nuclear export activity in HIV-1 matrix protein required for viral replication. Nature **402**:681–685.
60. **Gudleski N, Flanagan JM, Ryan EP, Bewley MC, Parent LJ.** 2010. Directionality of nucleocytoplasmic transport of the retroviral gag protein depends on sequential binding of karyopherins and viral RNA. Proc. Natl. Acad. Sci. U. S. A. **107**:9358–9363.
61. **Kemler I, Saenz D, Poeschla E.** 2012. Feline immunodeficiency virus gag is a nuclear shuttling protein. J. Virol. **86**:8402–8411.
62. **Mullers E, Stirnnagel K, Kaulfuss S, Lindemann D.** 2011. Prototype foamy virus gag nuclear localization: a novel pathway among retroviruses. J. Virol. **85**:9276–9285.
63. **Nash MA, Meyer MK, Decker GL, Arlinghaus RB.** 1993. A subset of Pr65gag is nucleus associated in murine leukemia virus-infected cells. J. Virol. **67**:1350–1356.
64. **Renault N, Tobaly-Tapiero J, Paris J, Giron ML, Coiffic A, Roingeard P, Saib A.** 2011. A nuclear export signal within the structural Gag protein is required for prototype foamy virus replication. Retrovirology **8**:6.
65. **Scheifele LZ, Garbitt RA, Rhoads JD, Parent LJ.** 2002. Nuclear entry and CRM1-dependent nuclear export of the Rous sarcoma virus Gag polyprotein. Proc. Natl. Acad. Sci. U. S. A. **99**:3944–3949.
66. **Parent LJ.** 2011. New insights into the nuclear localization of retroviral Gag proteins. Nucleus **2**:92–97.
67. **Garbitt-Hirst R, Kenney SP, Parent LJ.** 2009. Genetic evidence for a connection between Rous sarcoma virus gag nuclear trafficking and genomic RNA packaging. J. Virol. **83**:6790–6797.
68. **Warner JR, McIntosh KB.** 2009. How common are extraribosomal functions of ribosomal proteins? Mol. Cell **34**:3–11.
69. **Takagi M, Absalon MJ, McLure KG, Kastan MB.** 2005. Regulation of p53 translation and induction after DNA damage by ribosomal protein L26 and nucleolin. Cell **123**:49–63.
70. **Challagundla KB, Sun XX, Zhang X, DeVine T, Zhang Q, Sears RC, Dai MS.** 2011. Ribosomal protein L11 recruits miR-24/miRISC to repress c-Myc expression in response to ribosomal stress. Mol. Cell. Biol. **31**:4007–4021.
71. **Chen D, Zhang Z, Li M, Wang W, Li Y, Rayburn ER, Hill DL, Wang H, Zhang R.** 2007. Ribosomal protein S7 as a novel modulator of p53-MDM2 interaction: binding to MDM2, stabilization of p53 protein, and activation of p53 function. Oncogene **26**:5029–5037.
72. **Dai MS, Lu H.** 2004. Inhibition of MDM2-mediated p53 ubiquitination and degradation by ribosomal protein L5. J. Biol. Chem. **279**:44475–44482.
73. **Dai MS, Zeng SX, Jin Y, Sun XX, David L, Lu H.** 2004. Ribosomal protein L23 activates p53 by inhibiting MDM2 function in response to ribosomal perturbation but not to translation inhibition. Mol. Cell. Biol. **24**:7654–7668.
74. **Jin A, Itahana K, O'Keefe K, Zhang Y.** 2004. Inhibition of HDM2 and activation of p53 by ribosomal protein L23. Mol. Cell. Biol. **24**:7669–7680.
75. **Wanzel M, Russ AC, Kleine-Kohlbrecher D, Colombo E, Pelicci PG, Eilers M.** 2008. A ribosomal protein L23-nucleophosmin circuit coordinates Mizl function with cell growth. Nat. Cell Biol. **10**:1051–1061.
76. **Wan F, Anderson DE, Barnitz RA, Snow A, Bidere N, Zheng L, Hegde V, Lam LT, Staudt LM, Levens D, Deutsch WA, Lenardo MJ.** 2007. Ribosomal protein S3: a KH domain subunit in NF-kappaB complexes that mediates selective gene regulation. Cell **131**:927–939.
77. **Narla A, Ebert BL.** 2010. Ribosomopathies: human disorders of ribosome dysfunction. Blood **115**:3196–3205.
78. **Shenoy N, Kessel R, Bhagat T, Bhattacharya S, Yu Y, McMahon C,**

Verma A. 2012. Alterations in the ribosomal machinery in cancer and hematologic disorders. J. Hematol. Oncol. **5**:32.
79. **Amsterdam A, Sadler KC, Lai K, Farrington S, Bronson RT, Lees JA, Hopkins N.** 2004. Many ribosomal protein genes are cancer genes in zebrafish. PLoS Biol. **2**:e139. doi:10.1371/journal.pbio.0020139.
80. **Beck-Engeser GB, Monach PA, Mumberg D, Yang F, Wanderling S, Schreiber K, Espinosa R, III, Le Beau MM, Meredith SC, Schreiber H.** 2001. Point mutation in essential genes with loss or mutation of the second allele: relevance to the retention of tumor-specific antigens. J. Exp. Med. **194**:285–300.
81. **Lai K, Amsterdam A, Farrington S, Bronson RT, Hopkins N, Lees JA.** 2009. Many ribosomal protein mutations are associated with growth impairment and tumor predisposition in zebrafish. Dev. Dynamics **238**:76–85.
82. **Monach PA, Meredith SC, Siegel CT, Schreiber H.** 1995. A unique tumor antigen produced by a single amino acid substitution. Immunity **2**:45–59.
83. **Fukushi S, Okada M, Stahl J, Kageyama T, Hoshino FB, Katayama K.** 2001. Ribosomal protein S5 interacts with the internal ribosomal entry site of hepatitis C virus. J. Biol. Chem. **276**:20824–20826.
84. **Fok V, Mitton-Fry RM, Grech A, Steitz JA.** 2006. Multiple domains of EBER 1, an Epstein-Barr virus noncoding RNA, recruit human ribosomal protein L22. RNA **12**:872–882.
85. **Toczyski DP, Matera AG, Ward DC, Steitz JA.** 1994. The Epstein-Barr virus (EBV) small RNA EBER1 binds and relocalizes ribosomal protein L22 in EBV-infected human B lymphocytes. Proc. Natl. Acad. Sci. U. S. A. **91**:3463–3467.
86. **Blenis J, Erikson RL.** 1985. Regulation of a ribosomal protein S6 kinase activity by the Rous sarcoma virus transforming protein, serum, or phorbol ester. Proc. Natl. Acad. Sci. U. S. A. **82**:7621–7625.
87. **Maller JL, Foulkes JG, Erikson E, Baltimore D.** 1985. Phosphorylation of ribosomal protein S6 on serine after microinjection of the Abelson murine leukemia virus tyrosine-specific protein kinase into Xenopus oocytes. Proc. Natl. Acad. Sci. U. S. A. **82**:272–276.
88. **Kennedy IM, Leader DP.** 1981. Increased phosphorylation of ribosomal protein S6 in hamster fibroblasts transformed by polyoma virus and simian virus 40. Biochem. J. **198**:235–237.
89. **Bar-Sinai A, Bassa N, Fischette M, Gottesman MM, Love DC, Hanover JA, Hochman J.** 2005. Mouse mammary tumor virus Env-derived peptide associates with nucleolar targets in lymphoma, mammary carcinoma, and human breast cancer. Cancer Res. **65**:7223–7230.
90. **Dai MS, Shi D, Jin Y, Sun XX, Zhang Y, Grossman SR, Lu H.** 2006. Regulation of the MDM2-p53 pathway by ribosomal protein L11 involves a post-ubiquitination mechanism. J. Biol. Chem. **281**:24304–24313.